Structural Engineering and Mechanics, *Vol. 70, No. 2 (2019) 209-219*
DOI: https://doi.org/10.12989/sem.2019.70.2.209

Hysteresis characterization and identification of the normalized Bouc-Wen model

Zongjing Li[a] and Ganping Shu*

School of Civil Engineering, Southeast University, Nanjing 211189, China

(Received November 17, 2018, Revised February 13, 2019, Accepted February 20, 2019)

Abstract. By normalizing the internal hysteresis variable and eliminating the redundant parameter, the normalized Bouc-Wen model is considered to be an improved and more reasonable form of the Bouc-Wen model. In order to facilitate application and further research of the normalized Bouc-Wen model, some key aspects of the model need to be uncovered. In this paper, hysteresis characterization of the normalized Bouc-Wen model is first studied with respect to the model parameters, which reveals the influence of each model parameter to the shape of the hysteresis loops. The parameter identification scheme is then proposed based on an improved genetic algorithm (IGA), and verified by experimental test data. It is proved that the proposed method can be an efficacious tool for identification of the model parameters by matching the reconstructed hysteresis loops with the target hysteresis loops. Meanwhile, the IGA is shown to outperform the standard GA. Finally, a simplified identification method is proposed based on parameter sensitivity, which indicates that the efficiency of the identification process can be greatly enhanced while maintaining comparable accuracy if the low-sensitivity parameters are reasonably restricted to narrower ranges.

Keywords: Bouc-Wen model; hysteresis; characterization; identification; genetic algorithm

1. Introduction

Hysteresis behaviors as the intrinsic property of inelastic systems, are observed in structures and components subject to external excitations such as earthquakes, winds, recurrent waves, explosions and environmental vibration or shock. For a typical nonlinear single-degree-of-freedom(SDOF) system, the equation of motion can be expressed as

$$m\ddot{u}+c\dot{u}+R=p \tag{1}$$

where m and c represent the mass and the viscous damping coefficient, respectively. u, $\dot{u}$ and $\ddot{u}$ represent the displacement, velocity and acceleration, respectively. p represent the external excitation. R represents the nonlinear restoring force which can be described by a hysteresis model. A variety of such analytical models have been developed to describe hysteresis behaviors encountered in mechanics, civil engineering and many other related domains, such as ideal elasto-plastic model (Tena-Colunga 1997), bilinear model (Nakashima *et al.* 1995, Tena-Colunga 1997, Chen *et al.* 2006), multilinear model (Benavent-Climent 2010), Ramberg-Osgood model (Nakashima *et al.* 1995, Sireteanu *et al.* 2014), Bouc-Wen model (Chan *et al.* 2009, Sireteanu *et al.* 2014, Rahimi and Soltani 2017), Davidenkov model (Davidenkov 1939, Yang and Chen 1992), trace method model (Badrakhan 1987, Badrakhan 1988), Preisach model (Bolshakov and Lapovok 1996), etc., among which the Bouc-Wen Model has become one of the most widely accepted hysteresis models for nonlinear systems.

Originally proposed by Bouc (1967) and later generalized by Wen (1976), the classic Bouc-Wen model is a smooth analytical model described by differential equations, which can be used to describe a variety of hysteresis behaviors for structures and components made of different materials, such as steel frames (Hann *et al.* 2009), timber shear walls (Zhang *et al.* 2002), RC joints (Sengupta and Li), etc. Additionally, the Bouc-Wen model is especially popular in describing the force-displacement relationship of various energy dissipation devices for structural vibration control, such as BRBs (Black *et al.* 2004), metallic dampers (Shih and Sung 2005, Chan *et al.* 2009), MR dampers (Spencer *et al.* 1997) and isolation bearings (Alessandri *et al.* 2015, Chen *et al.* 2016), etc.

However, the classic Bouc-Wen Model is functionally redundant (Ma *et al.* 2004), i.e., a specific Bouc-Wen hysteresis curve does not correspond to a unique set of parameters, which means identification procedures that use input-output data cannot determine the parameters of the Bouc-Wen model. In order to eliminate the redundant parameter and facilitate the parameter identification procedure, a normalized form of the Bouc-Wen model was proposed by Ikhouane (2007). In this article, further studies are conducted for hysteresis characterization and identification of the normalized Bouc-Wen model. The remainder of the paper is organized as follows. In Section 2, the analytical expressions of the classic Bouc-Wen model and normalized Bouc-Wen model are introduced

*Corresponding author, Professor
E-mail: 230129153@seu.edu.cn, sgp0818@vip.sina.com
[a]Ph.D. Student

http://www.techno-press.com/journals/sem&subpage=7 ISSN: 1225-4568 (Print), 1598-6217 (Online)

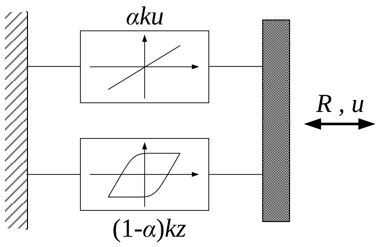

Fig. 1 Schematic diagram of the classic Bouc-Wen model

respectively. The relations between the normalized Bouc-Wen model parameters and corresponding hysteretic characteristics of the hysteresis loops described by the model are studied in Section 3. In Section 4, the parameter identification method is then proposed based on an improved genetic algorithm (IGA), and verified by experimental test data in Section 5. Additionally, a simplified identification method is proposed in Section 6 based on parameter sensitivity. Finally, a summary of findings is provided in Section 7.

2. Normalization of the Bouc-Wen model

2.1 The classic Bouc-Wen model

The classic Bouc-Wen model describes the hysteresis behavior of a nonlinear system in the form

$$R = \alpha ku + (1\text{-}\alpha)kz \tag{2a}$$

$$\dot{z} = A\dot{u} - \beta\left|\dot{u}\right|z\left|z\right|^{n-1} - \gamma\dot{u}\left|z\right|^{n} \tag{2b}$$

in which $\{R, z, u\}$ are the basic variables of the model, while $\{A, k, \alpha, \beta, \gamma, n\}$ are the parameters of the model. R, z and u represents the restoring force, internal hysteresis variable, and displacement, respectively. k controls the initial tangent stiffness, α governs the ratio of post-yield to pre-yield stiffness. A, β and γ are nondimensional parameters that control the shape of the hysteresis loop, while n is a positive scalar that decides the smoothness of transition from the elastic to the inelastic region. The overdot represents derivative with respect to time t. In addition, the initial value for z is 0, i.e., $z(0)=0$. A schematic diagram of the classic Bouc-Wen model is given in Fig. 1, which indicates that the total restoring force can be deemed as the parallel combination of an elastic component and a hysteretic component. Obviously, the restoring force is purely hysteretic if $\alpha=0$, or purely elastic if $\alpha=1$.

2.2 The normalized Bouc-Wen model

In order to eliminate the redundant parameter in the classic Bouc-Wen model, a new form of the Bouc-Wen model via normalizing the internal variable was proposed by Ikhouane (2007), which describes the hysteresis behavior of a nonlinear system in the form

$$R = k_u u + k_w w \tag{3a}$$

$$\dot{w} = \lambda(\dot{u} - \xi\left|\dot{u}\right|w\left|w\right|^{n-1} + (\xi - 1)\dot{u}\left|w\right|^{n}) \tag{3b}$$

in which $\{R, u, w\}$ are the basic variables of the model, while $\{k_u, k_w, \lambda, \xi, n\}$ are the parameters of the model. Furthermore, the relation between the two different forms of Bouc-Wen model is shown below

$$w = \frac{z}{z_0} \tag{4a}$$

$$z_0 = \left(\frac{A}{\alpha + \beta}\right)^{\frac{1}{n}} \tag{4b}$$

$$k_u = \alpha k \tag{4c}$$

$$k_w = (1\text{-}\alpha)kz_0 \tag{4d}$$

$$\lambda = \frac{A}{z_0} \tag{4e}$$

$$\xi = \frac{\beta}{\beta + \gamma} \geq 0 \tag{4f}$$

in which z_0 is the largest value of the internal hysteresis variable z, i.e., $|z|\leq z_0$. Considering Eq. (4a), we get $|w|\leq 1$. Thus, the internal hysteresis variable is scaled to unity, and w is named as the normalized internal hysteresis variable. In addition, the initial value for w is 0, i.e., $w(0)=0$. Instead of 6 parameters $\{A, k, \alpha, \beta, \gamma, n\}$ in the classic Bouc-Wen model, the normalized Bouc-Wen model has only 5 parameters $\{k_u, k_w, \lambda, \xi, n\}$. Meanwhile, the redundant parameter has been removed in the model (Ikhouane 2007), so that parameter identification can be implemented directly based on the normalized Bouc-Wen model. A schematic diagram of the normalized Bouc-Wen model is given in Fig. 2, which indicates that the total restoring force can be deemed as the parallel combination of an elastic component and a hysteretic component. Apparently, the model turns into a pure hysteretic system if $k_u=0$, or a pure elastic system if $k_w=0$.

3. Hysteresis characterization

Typical hysteresis loops described by the normalized Bouc-Wen model is shown in Fig. 3. Point O is the origin where the loop starts. Points A and B corresponding to the designed maximum positive and negative displacement respectively, are defined as the ‘shift point’ where the loading direction changes, i.e., the sign of the velocity $\dot{u}$ changes. Points Y^+ and Y^- are defined as the positive and negative ‘equivalent yield point’, which are the intersections of the elastic tangent lines from the origin point and the extension lines of the plastic stage. Displacement and restoring force corresponding to the ‘equivalent yield point’ is defined as the yield displacement u_y and yield force R_y. Slope of line $\overline{OY^+}$ and $\overline{OY^-}$ is defined as the initial elastic stiffness K_e, while slope of line $\overline{Y^+A}$ and $\overline{Y^-B}$ is defined as the plastic stiffness K_p. Those hysteresis characteristics directly related to the

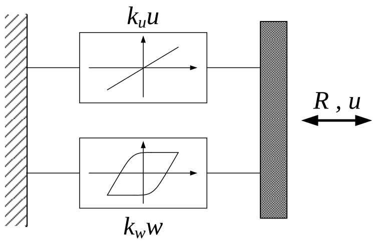

Fig. 2 Schematic diagram of the normalized Bouc-Wen model

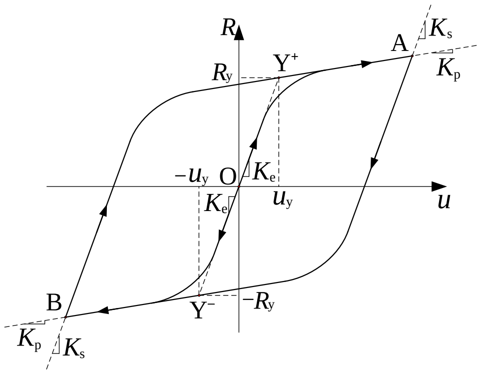

Fig. 3 Hysteretic characteristics of the normalized Bouc-Wen model

‘equivalent yield point’ are the critical indices for the evaluation of structures or components described by the Bouc-Wen model. Other hysteresis characteristics also include the shift stiffness K_s defined as the slope of the curve immediately after the shift-point, and the smoothness of transition from elastic to plastic response. In this section, the relations between the hysteretic characteristics and the parameters of the normalized Bouc-Wen model are studied first.

3.1 Initial elastic stiffness K_e

Differentiate Eq. (3a) with respect to time at t=0

$$\left.\frac{dR}{dt}\right|_{t=0} = k_u \left.\frac{du}{dt}\right|_{t=0} + k_w \left.\frac{dw}{dt}\right|_{t=0} \tag{5}$$

Using Eq. (3b) with $w(0)=0$, it leads to

$$\left.\frac{dw}{dt}\right|_{t=0} = \lambda \left.\frac{du}{dt}\right|_{t=0} \tag{6}$$

Combining Eq. (5) and (6), with $u(0)=0$, it follows that

$$\left.\frac{dR}{du}\right|_{u=0} = k_u + \lambda k_w \tag{7}$$

Thus, the slope of the w-u curve at origin point, i.e., the initial elastic stiffness K_e is obtained

$$K_e = k_u + \lambda k_w \tag{8}$$

3.2 Plastic stiffness K_p

Differentiate Eq. (3a) with respect to displacement with $u\to\infty$

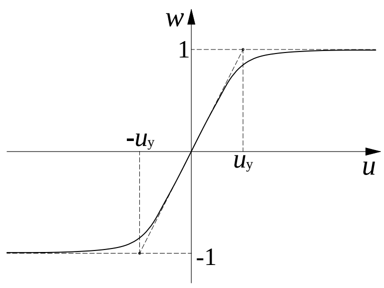

Fig. 4 Relation between w and u

$$\left.\frac{dR}{du}\right|_{u\to\infty} = k_u + k_w \left.\frac{dw}{du}\right|_{u\to\infty} \tag{9}$$

As u goes from zero to positive or negative infinity, the relation between w and u is shown in Fig. 4. As shown, w goes asymptotically to $w=\pm1$ as the displacement u goes to infinity. Accordingly, the slope of the w-u curve decreases asymptotically to zero as u approaches infinity, which gives

$$\left.\frac{dw}{du}\right|_{u\to\infty} = 0 \tag{10}$$

By substituting Eq. (10) into Eq. (9), we get

$$\left.\frac{dR}{du}\right|_{u\to\infty} = k_u \tag{11}$$

Therefore, the plastic stiffness K_p is obtained

$$K_p = k_u \tag{12}$$

3.3 Yield displacement u_y

Given that the restoring force of the normalized Bouc-Wen model is comprised of an elastic linear part $k_u u$ and a hysteretic nonlinear part $k_w w$, the yield displacement u_y is actually determined by the normalized internal hysteresis variable w.

The initial slope of the w-u curve at the origin point can be obtained by Eq. (3b) with $w(0)=0$ and $u(0)=0$, which gives

$$\left.\frac{dw}{du}\right|_{u=0} = \lambda \tag{13}$$

Therefore, the initial tangent line of the w-u curve is

$$w=\lambda u \tag{14}$$

As shown in Fig. 4, the ‘equivalent yield point’ for the w-u curve is the intersection of the initial tangent line $w=\lambda u$ and the asymptote $w=\pm1$. Thus, the corresponding displacement is the yield displacement of the nonlinear system

$$u_y = \frac{1}{\lambda} \tag{15}$$

3.4 Yield force R_y

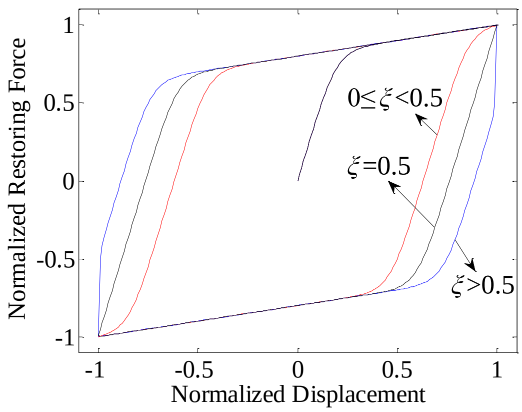

Fig. 5 Influence of ξ on the shift stiffness

The relation among the yield force R_y, the yield displacement u_y and the initial elastic stiffness K_e is as follows

$$R_y = K_e \cdot u_y \tag{16}$$

By substituting Eqs. (8) and (15) into Eq. (16), the yield force R_y is obtained

$$R_y = k_u/\lambda + k_w \tag{17}$$

3.5 Shift stiffness K_s

As shown in Fig. 3, $\dot{u} \cdot w < 0$ is satisfied after both the positive shift point A and the negative shift point B, with which Eq. (3b) can be revised as

$$\frac{dw}{dt} = \lambda \frac{du}{dt}[1-(1-2\xi)\cdot|w|^n] \tag{18}$$

Thus, we get the slope of the w-u curve after the shift points

$$\frac{dw}{du} = \lambda[1-(1-2\xi)\cdot|w|^n] \tag{19}$$

Differentiate Eq. (3a) with respect to displacement u

$$\frac{dR}{du} = k_u + k_w \frac{dw}{du} \tag{20}$$

By substituting Eq. (19) into Eq. (20), the shift stiffness K_s is obtained

$$K_s = k_u + \lambda k_w[1-(1-2\xi)\cdot|w|^n] \tag{21}$$

Comparing Eq. (21) with Eq. (8), the following conclusion can be drawn: if $0 \le \xi < 0.5$, $K_s < K_e$; if $\xi = 0.5$, $K_s = K_e$; if $\xi > 0.5$, $K_s > K_e$. The hysteresis loops of the normalized Bouc-Wen model with different values of ξ are shown in Fig. 5. Thus, we know that the relation between shift stiffness K_s and initial elastic stiffness K_e is decided by the parameter ξ in the model.

3.6 Transition from elastic to plastic response

A major difference between the bilinear model and the Bouc-Wen model is that the former simplifies the transition

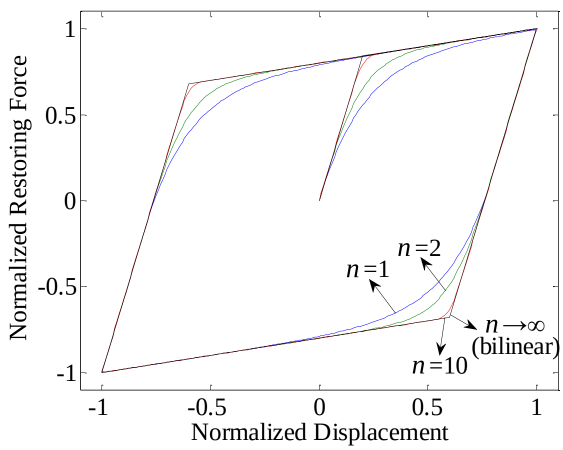

Fig. 6 Influence of n on the smoothness of transition

from elastic to plastic response to a single point, while the latter features a smooth transition from elastic to plastic response, which is more accordant with the actual conditions. Structures and components may exhibit different smoothness of transition due to various materials, forms of structure, and boundary conditions, etc. Thus, the transition is also an aspect of the hysteretic characteristics concerned.

As shown in Fig. 2, the restoring force defined by the normalized Bouc-Wen model is the parallel combination of an elastic linear component $k_u u$ and a nonlinear hysteretic component $k_w w$. Therefore, the transition is determined by the hysteretic component, i.e., the normalized internal variable w. Furthermore, the essence of the transition is actually the process that the slope of the w-u curve decrease from λ to 0, as shown in Fig. 4. As the transition only occurs when $\dot{u} \cdot w > 0$, according to Eq. (3b), the slope of the w-u curve during transition is

$$\frac{dw}{du} = \lambda[1-|w|^n] \tag{22}$$

Consider the process that w increases from 0 to 1 as shown in Fig. 4. Based on Eq. (22), if n is relatively small, the slope of the w-u curve decreases steadily as w increases. Thus, the transition tends to be smoother. If n is relatively large, the slope of the w-u curve stays almost unchanged when w is not near 1, and drops dramatically to 0 as w approaches near 1. Thus, the transition tends to be sharper. The transition of the normalized Bouc-Wen model with different values of n is shown in Fig. 6. Theoretically, when $n \to \infty$, the transition reduces to a sharp turning point, which made the normalized Bouc-Wen model equivalent to the bilinear model. Thus, we know that the smoothness of the transition is determined by the parameter n in the normalized Bouc-Wen model. Additionally, it should be noted that n needs to remain positive to avoid divergence of the solution.

4. Identification scheme

4.1 Definition and calculation of objective function

In order to identify the parameters of the normalized Bouc-Wen model based on a set of force-displacement test data, the error between the reconstructed hysteresis curves by the model and original hysteresis curves by the test needs to be minimized. Therefore, the parameter identification can be deemed as an optimization problem to minimize the objective function defined as

$$SSE = \sum_{i=1}^{N}(R_i^{\exp} - R_i^{\mathrm{sim}})^2 \tag{23}$$

where *SSE* represents the sum of squared error between the experimental data and the model simulation data. N is the total number of sampling points. $R_i^{\exp}$ is the restoring force of the ith sampling point in the test data, while R_i^{sim} is the restoring force of the ith sampling point in the simulation data.

When generating the simulation data using the model, there are generally two different situations regarding the type of the experimental test. For a displacement-controlled test, such as the pseudo-static loading test, the time history of displacement and its derivatives are readily available, so that the simulation data can be obtained directly by solving Eq. (3). For a force-controlled or acceleration-controlled test, such as the pseudo-dynamic test or the shaking-table test, the simulation data can be obtained by combining Eq. (1) and Eq. (3), then transforming the equations into a state-space form, and finally solving the simultaneous equations using first-order differential equation solvers, such as the Runge-Kutta method (Charalampakis and Koumousis 2008, Shampine and Reichelt 1997).

4.2 The improved genetic algorithm (IGA)

Genetic algorithms (GAs) are a class of meta-heuristic algorithms which can be used to generate high-quality solutions for a variety of optimization problems. The first genetic algorithm was originally proposed by Holland (1975), and then developed by Goldberg (1989). After years of efforts, the genetic algorithms have been widely accepted as a powerful optimization tool and applied to various domains (Dao *et al.* 2017). The basic idea of the genetic algorithms is based on Darwin's theory of natural selection and survival of the fittest. In a genetic algorithm, a population of individuals (i.e., candidate solutions) is randomly generated. After that, the population begins to evolve towards better solutions through the selection, crossover and mutation operators. During the process, the individuals with higher fitness (i.e., better solutions) have more chances to survive and pass their genes (i.e., characteristics) on to the next generation. Thus, an artificial system is modelled mathematically by emulating the real natural evolution.

In this paper, the genetic algorithm is adopted to identify the parameters of the normalized Bouc-Wen model in terms of minimizing the objective function *SSE*. The fitness function is defined as

$$fit = 1 - \sqrt{\frac{\sum_{i=1}^{N}(R_i^{\exp} - R_i^{\mathrm{sim}})^2}{\sum_{i=1}^{N}(R_i^{\exp})^2}} = 1 - \sqrt{\frac{SSE}{\sum_{i=1}^{N}(R_i^{\exp})^2}} \tag{24}$$

where $0 \leq fit \leq 1$. Consequently, the individuals with lower *SSE* would possess higher fitness value, and thus have more chances to survive during the selection operation. In order to enhance the efficiency and improve the results of the identification process, a real-coded GA with improved genetic operators, namely, the improved genetic algorithm (IGA) is proposed. The major modifications to the genetic algorithm adopted in the identification are as follows.

(1) Real coding

The traditional genetic algorithms used binary coding to represent information in the solutions. However, the parameters of the normalized Bouc-Wen model are real numbers. Due to the mechanism of conversion from binary codes to real numbers, excessive length of binary coding strings may be needed in order to achieve satisfactory precision, which may largely increase the complexity and therefore affect the efficiency of the algorithm. Instead, real coding can be used as a good alternative. Meanwhile, the decoding procedure is eliminated when encoding with real numbers. Thus, the coding strategy used in this paper is (G_1, G_2, G_3, G_4, G_5), where G_i is a real number representing the value of the ith parameter of the normalized Bouc-Wen model.

(2) Adjustable tournament size in the selection operator

The roulette wheel selection is a traditional and commonly used strategy for the selection operator. However, a premature convergence is likely to occur when using the roulette wheel selection because the probability of selection is directly proportionate to the fitness value of each individual. A preferable alternative to avoid premature convergence caused by the selection operator is to use the tournament selection strategy, which runs a "tournament" among a few individuals randomly chosen from the population and selects the winner with the best fitness value for crossover. The number of individuals which take part in the tournament is defined as the tournament size k. As a result, the probability of selection for each individual is not directly proportionate to its fitness value, so that premature convergence can be effectively avoided with respect to the selection operator.

Furthermore, the selection pressure can be adjusted through the tournament size k (Alcan and Başlıgil 2012). If the tournament size is larger, weak individuals have a smaller chance to be selected, which may be explained that when a weak individual is selected to be in a tournament, there is a higher probability that a stronger individual is also in that tournament when the tournament size is larger. In the early phase of evolution, a smaller tournament size is preferable in order to maintain diversity in the population so that the solution space can be further explored, while in the final phase of evolution, when the difference among the fitness values of individuals are getting smaller, a larger tournament size is preferable in order to raise the selection pressure so that better individuals may stand out more easily during selection. Therefore, in this study, the tournament size is suggested to be adjustable, i.e., smaller in the early phase and larger in the final phase.

(3) Adaptive crossover and mutation rates in the crossover and mutation operators

Crossover rate p_c and mutation rate p_m are fixed in the

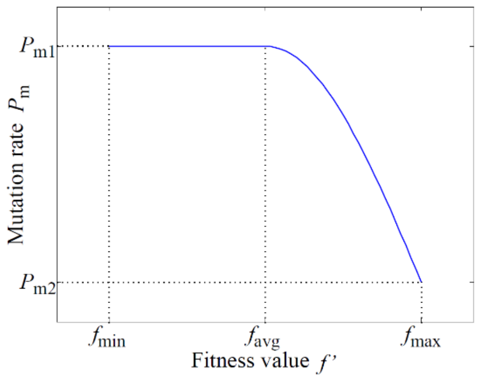

(a) P_c v.s. f

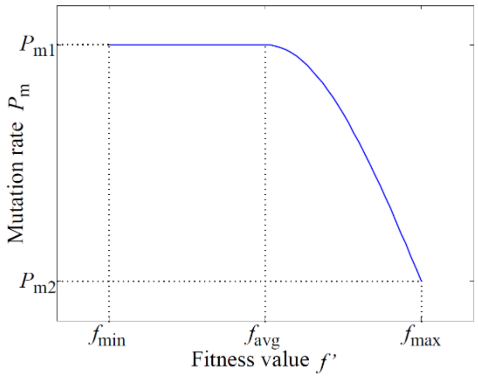

(b) P_m v.s. f'

Fig. 7 Adaptive crossover and mutation rates

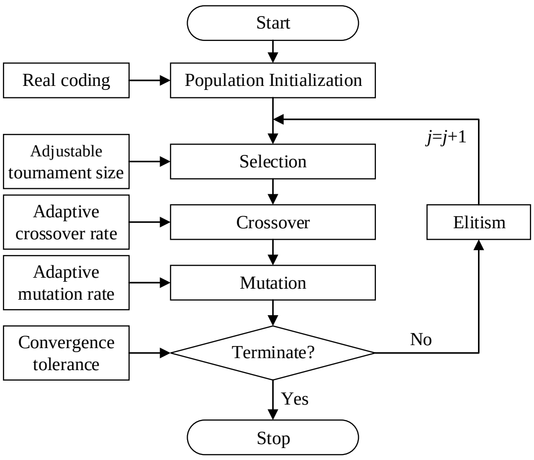

Fig. 8 Flow chart of the improved genetic algorithm (IGA)

traditional GA. Srinivas (1994) proposed a theory of adaptive rates of crossover and mutation, in which p_c and p_m are not fixed but dependent on the fitness value as follows

$$P_c = \begin{cases} P_1(f_{max} - f)/(f_{max} - f_{avg}), & \text{if } f \geq f_{avg} \\ P_2, & \text{if } f < f_{avg} \end{cases} \tag{25}$$

$$P_m = \begin{cases} P_3(f_{max} - f')/(f_{max} - f_{avg}), & \text{if } f' \geq f_{avg} \\ P_4, & \text{if } f' < f_{avg} \end{cases} \tag{26}$$

where P_1, P_2, P_3 and P_4 are predefined constants between 0 and 1. f_{max} is the maximum fitness value of the population,

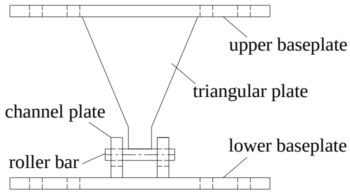

(a) front view

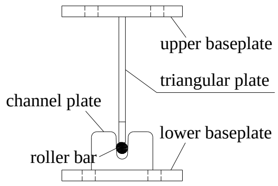

(b) side view

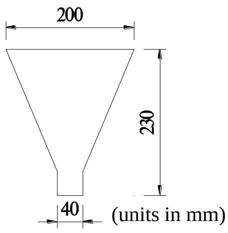

(c) size of the triangular plate

Fig. 9 Diagram of the TADAS element

while f_{avg} is the average fitness value of the population. f is the larger of the fitness value of the individuals to be crossed, while f' is the fitness value of the individual to be mutated. As a result, p_c and p_m will be lower for better individuals, and higher for weaker individuals. In addition, when the differences between individuals tend to diminish, i.e., the gap between the maximum and average fitness value is narrowed down, the proposed mechanism automatically favors higher crossover and mutation rates. Thus, a trade-off between exploitation of the optimal solution and exploration of the solution space is maintained.

However, according to Eqs. (25) and (26), the crossover and mutation rates of the best individuals are close to 0, which prevents the good individuals from further improvements, and is unfavorable in the early phase of the evolution. Therefore, further improvements are made, and the crossover and mutation rates in this study are modified as follows

$$P_c = \begin{cases} P_{c2} + (P_{c1} - P_{c2}) \cdot \cos\left(\dfrac{f - f_{avg}}{f_{max} - f_{avg}} \cdot \dfrac{\pi}{2}\right), & \text{if } f \geq f_{avg} \\ P_{c1}, & \text{if } f < f_{avg} \end{cases} \tag{27}$$

$$P_m = \begin{cases} P_{m2} + (P_{m1} - P_{m2}) \cdot \cos\left(\dfrac{f' - f_{avg}}{f_{max} - f_{avg}} \cdot \dfrac{\pi}{2}\right), & \text{if } f' \geq f_{avg} \\ P_{m1}, & \text{if } f' < f_{avg} \end{cases} \tag{28}$$

where P_{c1} and P_{c2} are the upper and lower bounds of the probability of crossover respectively. P_{m1} and P_{m2} are the upper and lower bounds of the probability of mutation respectively. By adopting the modified adaptive crossover and mutation rates, P_c and P_m of the best individuals are P_{c2} and P_{m2}, respectively. The relationship between P_c and f, as well as P_m and f', can be draw in Fig. 7.

(4) Termination criteria

The simplest way to terminate the implementation of GA is to set a maximum number of iterations. However, it is hard to determine the proper number of iterations needed to generate a satisfying solution in advance. Alternatively, a more reasonable way for termination of GA is to set a convergence tolerance ε. When the improvements of the best fitness value remain less than ε over a fixed number of iterations, the termination order is executed.

In addition, previous studies have shown that the elitism scheme may enhance the performance of GA significantly (Deb *et al.* 2002, Zitzler *et al.* 2014). Therefore, elitism is built into the proposed IGA in this study which copies the best individual so far into the next generation in each iteration, to ensure survival of the best individual in subsequent generations. Furthermore, after the parameters of the normalized Bouc-Wen model have been identified, the corresponding hysteretic characteristics can be obtained by equations provided in Section 3. The flow chart of the entire process for parameter identification is shown in Fig. 8, which is implemented through Matlab code.

5. Identification using experimental test data

5.1 Test setup and original data

The TADAS device (Tsai *et al.* 1993, Saeedi *et al.* 2016, Mohagheghian and Mohammadi 2017) is a typical energy dissipation component for structural vibration control whose hysteresis behavior can be described by the Bouc-Wen model. By installing the TADAS device in the structure, a large amount of earthquake input energy can be dissipated through the uniformly distributed plastic deformation on the steel triangular plates of the TADAS device. As a result, the dynamic response of the structure can be effectively reduced under seismic excitation.

The TADAS device is composed of multiple pieces of TADAS elements in parallel. In order to investigate the hysteretic performance and evaluate the hysteretic characteristics of the TADAS element, a displacement-controlled pseudo-static cyclic loading test was carried out in the structural engineering laboratory at Southeast University, based on which the implementation and effectiveness of the proposed identification method can be further verified. Details of the TADAS element are shown in Fig. 9, which is mainly consisted of a triangular plate for energy dissipation, an upper baseplate and a lower baseplate for connection with the main structure, and two channel plates with slotted holes. The upper end of the triangular plate is welded to the upper baseplate, while the lower end is welded to a roller bar, which is inserted into the slotted holes of the channel plates during assembly, as shown in Fig. 10. As a result, the upper boundary condition for the triangular plate is fixed, while the lower boundary condition is pinned. The triangular plate was made of 12 mm thick Q345 steel, whose nominal yield strength is 345 N/mm^2. The schematic of the test setup is shown in Fig. 11. As

(a) front view

(b) side view

Fig. 10 Picture of the TADAS element

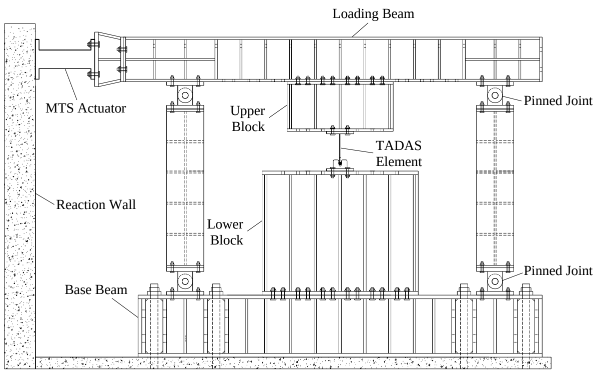

Fig. 11 Schematic diagram of the test setup

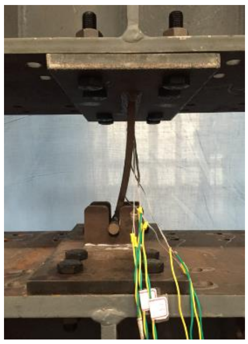

Fig. 12 Deformed TADAS element

shown, the TADAS element was installed between an upper block and a lower block in a pinned frame. As the actuator pulls/pushes the loading beam horizontally, the displacement (i.e. the inter-story drift) can be effectively imposed on the TADAS element. Similar test setups were also adopted in the experimental studies of various steel dampers conducted by Deng (2015) and Xu (2016). Deformation of the TADAS element during the cyclic loading is shown in Fig. 12. Displacement and force were

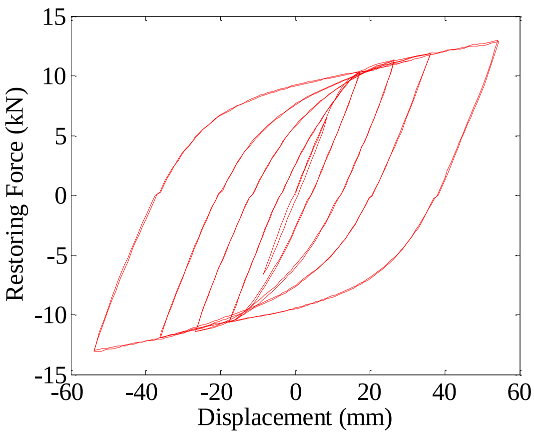

Fig. 13 Hysteresis curves of the TADAS element by test data

measured during the cyclic loading process, from which the experimental hysteresis curves can be draw, as shown in Fig. 13.

5.2 Implementation of identification

The identification was implemented according to the procedures shown in Fig. 9 with the following configurations: population size N_{pop}=40; initial tournament size k_0=2 in the first 80 generations, with an increment of 1 in each subsequent 40 generations; upper and lower bounds of the crossover rates P_{c1}=0.9 and P_{c2}=0.6; upper and lower bounds of the mutation rates P_{m1}=0.5 and P_{m2}=0.05. The convergence tolerance was set as ε=0.001. The iteration was terminated if the improvements of the best fitness value remains less than ε over 30 consecutive iterations. Additionally, in order to verify the stability of the algorithm, another three trials of identification were implemented by varying the tournament size, crossover rate and mutation rate.

Comparison of the original hysteresis curves by experimental data and the reconstructed hysteresis curves by model simulation is presented in Fig. 14, in which the model simulation data is based on the identified results of the best trial with the highest fitness. Satisfactory agreement is reached between the original hysteresis curves and the reconstructed hysteresis curves. The iteration curves and identification results of the four consecutive trials of identification are shown in Fig. 15 and Table 1, respectively. The value of the fitness function remained almost unchanged over the four trials, which validates the stability of the algorithm. In addition, key hysteretic characteristics of the TADAS element can be obtained according to Eqs. (8), (12), (15), (17) given in Section 3, which leads to K_e=0.66 kN/mm, K_p=0.068 kN/mm, u_y=15.63 mm, R_y=10.38kN. Thus, the identification and evaluation for the tested sample of TADAS element are completed. Furthermore, standard genetic algorithm(SGA) including elitism scheme, with roulette wheel selection, fixed P_c and P_m, is also used to implement the identification for comparison, which yields a result of k_u=0.076, k_w=8.87, λ=0.0726, ξ=0.680, n=4.06. The corresponding fitness value

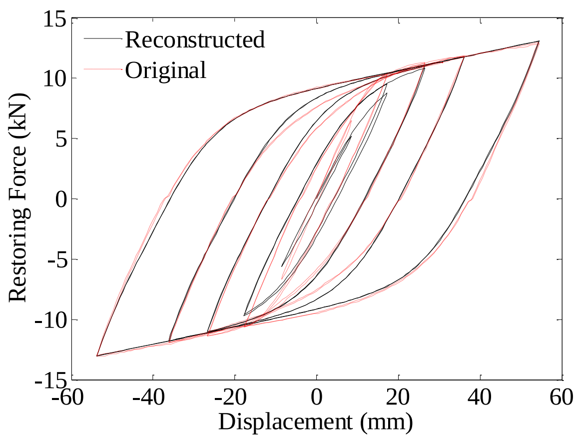

Fig. 14 Original and reconstructed hysteresis curves

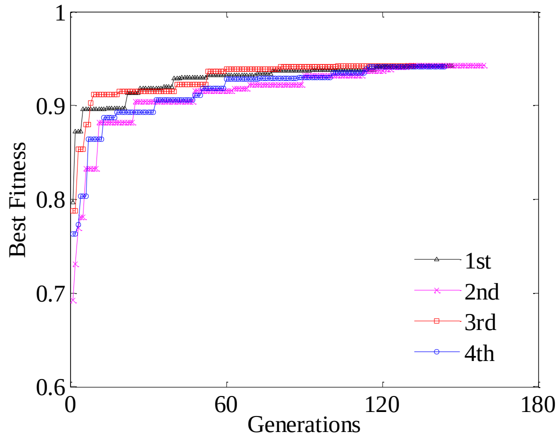

Fig. 15 Iteration curves of identification process

Table 1 Parameter identification results

Trial No.	Parameters of normalized Bouc-Wen model					Fitness function
	k_u (kN/mm)	k_w (kN)	λ (mm^{-1})	ξ	n	*fit*
1st	0.067	9.26	0.064	0.752	2.64	0.942
2nd	0.068	9.32	0.064	0.771	2.32	0.943
3rd	0.070	9.15	0.065	0.785	2.47	0.942
4th	0.068	9.38	0.063	0.843	1.86	0.941
Average	0.068	9.28	0.064	0.789	2.44	0.941
Max relative deviation*	4.40%	2.48%	3.13%	11.55%	33.58%	0.21%

*Max relative deviation is defined as the ratio of the difference between the maximum value and the minimum value to the average value, i.e., (Max-Min)/Average.

is *fit*=0.920, notably less than the results obtained by IGA. Therefore, the SGA may easily get trapped in local minima, while the IGA shows better robustness and effectiveness in the identification.

6. Simplified identification based on parameter sensitivity

It is noticed from Table 1 that the identification results

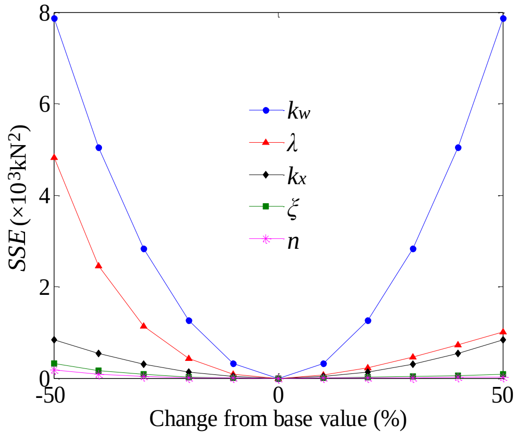

(a) *SSE* as sensitivity index

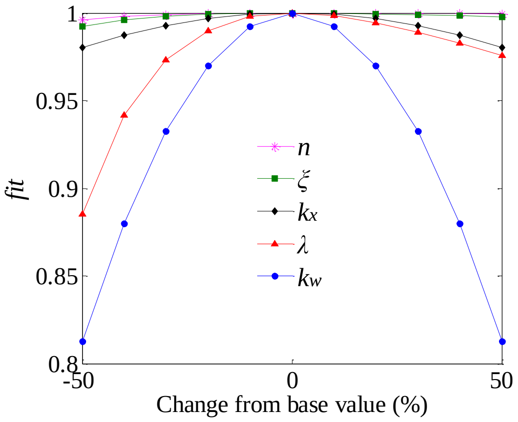

(b) *fit* as sensitivity index

Fig. 16 Spider diagram of parameter sensitivity

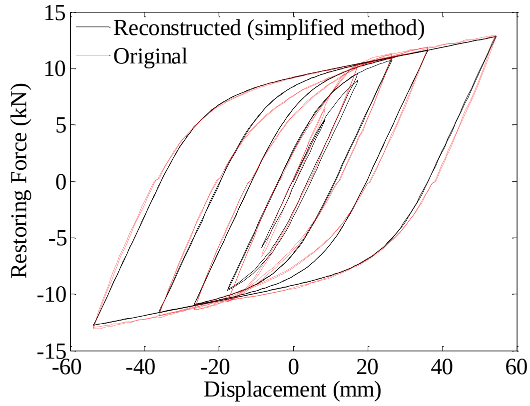

(a) Original and reconstructed hysteresis curves

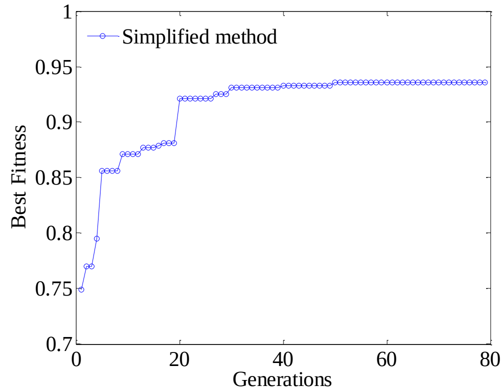

(b) Iteration curve

Fig. 17 Hysteresis curves and iteration curve by simplified identification

of k_u, k_w, and λ are stable over the four trials, whose max relative deviations are all within 5%, while the identification results of ξ and n vary from each trial, whose max relative deviations go beyond 10% and 30% respectively. However, the values of the fitness function are almost the same over the four trials. A possible reason may be explained that the objective function and the fitness function are more sensitive to the variance of k_u, k_w, and λ, while less sensitive to the variance of ξ and n. In order to verify the supposition, a parameter sensitivity study need to be conducted.

6.1 Parameter sensitivity

Typical methods for parameter sensitivity analysis can be categorized into either "local sensitivity analysis" or "global sensitivity analysis" (Hamby 1994). The local sensitivity analysis is implemented by repeatedly varying one parameter at a time while holding the others fixed at chosen nominal base values, which is the simplest and most commonly used way to conduct parameter sensitivity analysis. It is also referred to as the one-factor-at-a-time method (Ma *et al.* 2004).

In this paper, parameter sensitivity analysis is conducted through the one-factor-at-a-time method, with the base values chosen as $\{k_u, k_w, \lambda, \xi, n\}$={0.1 kN/mm, 10 kN, 0.1 mm^{-1}, 0.5, 2}. Each parameter is varied ±10%, ±20%, ±30%, ±40% and ±50% from its base value, and the objective function *SSE* defined by Eq. (23) and the fitness function *fit* defined by Eq. (24) are chosen as the sensitivity indices. The base values are used to calculate $R_i^{\exp}$, while the varied values are used to calculate R_i^{sim}. The hysteresis behavior is evaluated for a full cycle using the base and varied parameter sets, with the displacement amplitude set as ±50 mm, and the total number of sampling points set as N=400.

Spider diagrams are obtained by plotting the sensitivity indices against the varied percentages of each parameter as shown in Fig. 16. The results show that ξ and n exhibit obviously lower sensitivity than k_w, k_u and λ. Since the variance of ξ and n has only a minor influence on *SSE* and *fit*, and thus has a minor influence on the offset of the hysteresis curves, they can be categorized as the low-sensitivity parameters.

6.2 Simplified identification

Given that the low-sensitivity parameters have relatively smaller influence on the value of the objective function and the fitness function, the efficiency of the identification process can be further enhanced by narrowing down the search ranges and relaxing the accuracy requirements of the low-sensitivity parameters based on the specific conditions. Practically, very sharp transitions are rarely observed in the hysteresis curves of metallic energy dissipaters like the

TADAS device. Thus, the actual upper limit for n can be set as 10. Moreover, minor changes of n wouldn't cause obvious change to the hysteresis curves. Therefore, n can be set as an integer number instead of a real number. Hence, the search range for n in the parameter identification of normalized Bouc-Wen model for the TADAS element may be narrowed down to integer numbers between 1 and 10. In addition, the shift stiffness K_s is normally very close to the elastic stiffness K_e for the TADAS device. Thus, according to Eq. (21), the search range for ξ may be narrowed down to the neighborhood of 0.5, or even be directly set as 0.5 in the simplified identification method.

Once more the identification was implemented according to the aforementioned simplified identification method, in which the parameters to be identified are reduced to $\{k_u, k_w, \lambda, n\}$ by setting ξ=0.5 in advance, and the search range for n is further narrowed down to integers within [1, 10]. The hysteresis curves and iteration curves by the simplified identification method are shown in Fig. 17. Compared with the iteration curves in Fig. 15, it is shown that the convergence rate is greatly enhanced. The final identified results of the parameters are k_u=0.065 kN/mm, k_w=9.28 kN, λ=0.068 mm^{-1}, ξ=0.5, n=2, and the fitness value for the final solution is *fit*=0.936, which is just slightly less than that before simplification. Therefore, the balance between the quality of the results and the efficiency of the algorithm can be achieved through the simplified identification method by reasonably restricting the low-sensitivity parameters to narrower ranges and properly relaxing the accuracy requirements of the low-sensitivity parameters.

7. Conclusions

This paper reveals the relations between the normalized Bouc-Wen model parameters $\{k_w, k_u, \lambda, \xi, n\}$ and the corresponding hysteretic characteristics, i.e., the initial elastic stiffness K_e, plastic stiffness K_p, yield displacement u_y, yield force R_y, shift stiffness K_s and smoothness of transition from elastic to plastic response. The proposed parameter identification method based on the improved genetic algorithm (IGA) can effectively identify the parameters of the normalized Bouc-Wen model, and the simulated curves based on the identification results agree well with the hysteresis loops by the experiment. Furthermore, it is indicated that the efficiency of the identification process can be greatly enhanced without noticeably degrading the quality of the solution by reasonably restricting the low-sensitivity parameters to narrower ranges. The products of the study can provide effective reference for the application of the normalized Bouc-Wen model. However, it should be noted that the normalized Bouc-Wen model in the present study does not include pinching, degrading or other additional effects. In order to describe and evaluate hysteretic behaviors for a broader range of structures and components, more advanced forms of the normalized Bouc-Wen model are to be studied in the future researches.

Acknowledgments

This work is supported by the National Key Technology R&D Program of China during the 12th Five-Year Plan Period (No. 2012BAJ13B01-4); the Research and Innovation Project for College Graduates of Jiangsu Province (No. CXZZ13-0108); the Fundamental Research Funds for the Central Universities (No.3205004902).

References

Alcan, P. and Başlıgil, H. (2012), "A genetic algorithm application using fuzzy processing times in non-identical parallel machine scheduling problem", *Adv. Eng. Softw.*, **45**(1), 272-280.

Alessandri, S., Giannini, R., Paolacci, F. and Malena, M. (2015), "Seismic retrofitting of an HV circuit breaker using base isolation with wire ropes. Part 1: Preliminary tests and analyses", *Eng. Struct.*, **98**, 251-262.

Badrakhan, F. (1987), "Rational study of hysteretic systems under stationary random excitation", *Int. J. Nonlin. Mech.*, **22**(4), 312-325.

Badrakhan, F. (1988), "Dynamic analysis of yielding and hysteretic system by polynomial approximation", *J. Sound Vibr.*, **125**(1), 23-42.

Benavent-Climent, A. (2010), "A brace-type seismic damper based on yielding the walls of hollow structural sections", *Eng. Struct.*, **32**(4), 1113-1122.

Black, C.J., Makris, N. and Aiken, I.D. (2004), "Component testing, seismic evaluation and characterization of buckling-restrained braces, *J. Struct. Eng.*, **130**(6), 880-894.

Bolshakov, G.V. and Lapovok, A.J. (1996), "A Preisach model for magnetoelastic hysteresis", *J. Magn. Magn. Mater.*, **162**(1), 112-116.

Bouc, R. (1967), "Forced vibration of mechanical systems with hysteresis", *Proceedings of the 4th Conference on Nonlinear Oscillation*, Prague, Czechoslovakia.

Chan, R.W.K., Albermani, F. and Williams, M.S. (2009), "Evaluation of yielding shear panel device for passive energy dissipation", *J. Constr. Steel Res.*, **65**(2), 260-268.

Charalampakis, A.E. and Koumousis, V.K. (2008), "Identification of Bouc-Wen hysteretic systems by a hybrid evolutionary algorithm", *J. Sound Vibr.*, **314**(3), 571-585.

Chen, X., Li, J., Li, Y. and Gu, X. (2016), "Lyapunov-based semi-active control of adaptive base isolation system employing magnetorheological elastomer base isolators", *Earthq. Struct.*, **11**(6), 1077-1099.

Chen, Z., Ge, H. and Usami, T. (2006), "Hysteretic model of stiffened shear panel dampers", *J. Struct. Eng.*, **132**(3), 478-483.

Dao, S.D., Abhary, K. and Marian, R. (2017), "A bibliometric analysis of genetic algorithms throughout the history", *Comput. Ind. Eng.*, **110**, 395-403.

Davidenkov, N.N. (1939), "Hysteretic property of the ferrous metal", *Tech. Phys.*, **8**, 483-489.

Deb, K., Pratap, A., Agarwal, S. and Meyarivan, T. (2002), "A fast and elitist multiobjective genetic algorithm: NSGA-II", *IEEE Trans. Evol. Comput.*, **6**(2), 182-197.

Deng, K., Pan, P., Li, W. and Xue, Y. (2015), "Development of a buckling restrained shear panel damper", *J. Constr. Steel Res.*, **106**, 311-321.

Goldberg, D.E. (1989), *Genetic Algorithms in Search, Optimization, and Machine Learning*, Addison-Wesley, New York, U.S.A.

Hamby, D.M. (1994), "A review of techniques for parameter sensitivity analysis of environmental models", *Environ. Monit. Assess.*, **32**(2), 135-154.

Hann, C.E., Singh-Levett, I., Deam, B.L., Mander, J.B. and Chase, J.G. (2009), "Real-time system identification of a nonlinear four-story steel frame structure-application to structural health monitoring", *IEEE Sens. J.*, **9**(11), 1339-1346.

Holland, J.H. (1975), *Adaptation in Natural and Artificial Systems*, University of Michigan Press, Ann Arbor, Michigan, U.S.A.

Ikhouane, F. and Rodellar, J. (2007), *Systems with Hysteresis: Analysis, Identification and Control Using the Bouc-Wen Model*, John Wiley & Sons, Ltd., Chichester, West Sussex, U.K.

Ma, F., Zhang, H., Bockstedte, A., Foliente, G.C. and Paevere, P. (2004), "Parameter analysis of the differential model of hysteresis", *J. Appl. Mech.-Trans. ASME*, **71**(3), 342-349.

Mohagheghian, K. and Mohammadi, R.K. (2017), "Comparison of online model updating methods in pseudo-dynamic hybrid simulations of TADAS frames", *Bull. Earthq. Eng.*, **15**(10), 1-22.

Nakashima, M., Akazawa, T. and Tsuji, B. (1995), "Strain-hardening behavior of shear panels made of low-yield steel. II: model", *J. Struct. Eng.*, **121**(12), 1750-1757.

Rahimi, S. and Soltani, M. (2017), "Expected extreme value of pounding force between two adjacent buildings", *Struct. Eng. Mech.*, **61**(2), 183-192.

Saeedi, F., Shabakhty, N. and Mousavi, S.R. (2016), "Seismic assessment of steel frames with triangular-plate added damping and stiffness devices", *J. Constr. Steel Res.*, **125**, 15-25.

Sengupta, P. and Li, B. (2013), "Modified Bouc-Wen model for hysteresis behavior of RC beam-column joints with limited transverse reinforcement", *Eng. Struct.*, **46**, 392-406.

Shampine, L.F. and Reichelt, M.W. (1997), "The MATLAB ODE Suite", *SIAM J. Sci. Comput.*, **18**(1), 1-22.

Shih, M.H. and Sung, W.P. (2005), "A model for hysteretic behavior of rhombic low yield strength steel added damping and stiffness", *Comput. Struct.*, **83**(12-13), 895-908.

Sireteanu, T., Mitu, A.M., Giuclea, M. and Solomon, O. (2014), "A comparative study of the dynamic behavior of Ramberg-Osgood and Bouc-Wen hysteresis models with application to seismic protection devices", *Eng. Struct.*, **76**, 255-269.

Spencer, B.F., Dyke, S.J., Sain, M.K. and Carlson, J.D. (1997), "Phenomenological model of a magnetorheological damper", *J. Eng. Mech.*, **123**(3), 230-238.

Srinivas, M. and Patnaik, L.M. (1994), "Adaptive probabilities of crossover and mutation in genetic algorithms", *IEEE Trans. Syst. Man Cybern.*, **24**(4), 656-667.

Tena-Colunga, A. (1997), "Mathematical modelling of the ADAS energy dissipation device", *Eng. Struct.*, **19**(10), 811-821.

Tsai, K.C., Chen, H.W., Hong, C.P. and Su, Y.F. (1993), "Design of steel triangular plate energy absorbers for seismic-resistant construction", *Earthq. Spectr.*, **9**(3), 505-528.

Wen, Y.K. (1976), "Method for random vibration of hysteretic systems", *J. Eng. Mech.*, **102**(2), 249-263.

Xu, L.Y., Nie, X., Fan, J.S. (2016), "Cyclic behaviour of low-yield-point steel shear panel dampers", *Eng. Struct.*, **126**, 391-404.

Yang, S. and Chen, Y. (1992), "The bifurcations and singularities of the parameterical vibration in a system with Davidenkov's hysteretic nonlinearity", *Mech. Res. Commun.*, **19**(4), 267-272.

Zhang, H., Foliente, G.C., Yang, Y. and Ma, F. (2002), "Parameter identification of inelastic structures under dynamic loads", *Earthq. Eng. Struct. Dyn.*, **31**(5), 1113-1130.

Zitzler, E., Deb, K. and Thiele, L. (2014), "Comparison of multiobjective evolutionary algorithms: Empirical results", *Evol. Comput.*, **8**(2), 173-195.

CC